Effect of dynamical screening in the Bethe-Salpeter framework: Excitons in crystalline naphthalene

Xiao Zhang [1,*], Joshua A. Leveillee [2,†] and André Schleife [2,3,4,‡]

[1]*Department of Mechanical Science and Engineering, University of Illinois at Urbana-Champaign, Urbana, Illinois 61801, USA*
[2]*Department of Materials Science and Engineering, University of Illinois at Urbana-Champaign, Urbana, Illinois 61801, USA*
[3]*Materials Research Laboratory, University of Illinois at Urbana-Champaign, Urbana, Illinois 61801, USA*
[4]*National Center for Supercomputing Applications, University of Illinois at Urbana-Champaign, Urbana, Illinois 61801, USA*

Solving the Bethe-Salpeter equation (BSE) for the optical polarization functions is a first principles means to model optical properties of materials including excitonic effects. One almost ubiquitously used approximation neglects the frequency dependence of the screened electron-hole interaction. This is commonly justified by the large difference in the magnitude of electronic plasma frequency and exciton binding energy. We incorporated dynamical effects into the screening of the electron-hole interaction in the BSE using two different approximations as well as exact diagonalization of the exciton Hamiltonian. We compare these approaches for a naphthalene organic crystal, for which the difference between exciton binding energy and plasma frequency is only about a factor of ten. Our results show that in this case, corrections due to dynamical screening are about 15% of the exciton binding energy. We analyze the effect of screening dynamics on optical absorption across the visible spectral range and use our data to establish an *effective* screening model as a computationally efficient approach to approximate dynamical effects in complex materials in the future.

I. INTRODUCTION

Linear dielectric response is the underlying property that renders materials interesting for optoelectronic applications including solar cells, transistors, and displays, since excitations of electrons control fundamental mechanisms of optical absorption and emission [1–4]. Most state-of-the-art devices rely on traditional inorganic semiconductors that are well-studied from both experimental and theoretical perspective [5]. Apart from these, systems such as organic crystals have also been reported to have great potential, e.g., as solar cells, sensors, transistors, and others [6–10]. Singlet-triplet fission, for instance, can provide a novel mechanism that may enable design of more efficient, flexible solar cells [7,8]. It is thus important to accurately model optical and excitonic properties for these materials, to make reliable predictions for potential applications and device design.

Predictive first-principles simulations based on density functional theory (DFT) [11,12] and Fermi's golden rule have proven to be important in understanding optical absorption of many semiconductor materials [3,4,13,14]. However, the lack of considering the electron-hole Coulomb interactions that dominate excited electronic states render traditional DFT-based techniques insufficient for describing optical absorption. The independent-particle picture fails to provide accurate optical spectra and, in particular, does not provide information about excitonic effects that are critically important for applications, including organic solar cells [15–17]. To accurately model these, the *screened* Coulomb interaction of excited electron-hole pairs needs to be considered and the Bethe-Salpeter equation (BSE) approach within many-body perturbation theory is commonly used [4,18]. The solution of the BSE is a Green's function technique that allows to include excitonic effects in the first-principles description, leading to an accurate and commonly used theoretical-spectroscopy route to describe optical excitations. It has proven successful in many studies that predict optical and excitonic properties of bulk semiconductors [19–23].

Within the BSE approach, the accurate description of dielectric screening is an important aspect of the underlying physics that is key to accurately simulating optical spectra. While the screening of the electron-hole interaction is spatially inhomogeneous and dynamical in principle, especially the dynamical effects are not well explored in practice. This is because the theoretical description of dynamical screening is challenging, the computational cost is high, and such effects are believed to be small in many traditional bulk semiconductors. Hence, most of the BSE implementations currently used adopt a static, frequency-independent approximation of dielectric screening [23–28]. This approximation neglects the rearrangement of the electrons upon forming electron-hole pairs, i.e., the dynamical evolution of the screening [18].

Whether *electronic* screening dynamics can be neglected, however, is related to the relative ratio of the plasma frequency and the exciton binding energy of a material [4,18]. In particular, electronic dynamical effects cannot be neglected when exciton-binding energies are comparable to the

---

235205-1

plasma frequency. Examples of large exciton binding energies on the order of few hundreds of meV to a few eV include low-dimensional materials [29–32] and organic crystals [15–17,33]. Consequently, there are indeed computational studies of organic crystals and doped 2D materials [30,34] that report large corrections on the order of a few hundred meV for the exciton binding energy due to electronic screening dynamics. However, different approximations of incorporating dynamical screening effects, treating the dynamical screening as a first-order perturbation [4] or using an effective static screening function [30], have not been systematically compared to each other or to exactly solving the dynamical BSE.

In this work, we discuss different approximations for incorporating dynamical screening into the solution of the BSE. The challenges are at least twofold: dynamical screening of the electron-hole interaction complicates the many-body perturbation theory framework, since the resulting BSE depends on two frequencies, preventing a closed-form equation for a single-frequency dependent polarization function [4,18,35]. While this can be overcome using the Shindo approximation [18,36], the resulting BSE eigenvalue problem parametrically depends on the frequency and requires sampling of many frequency points, significantly increasing the computational cost. Rohlfing and Louie proposed a perturbative treatment and used it to examine dynamical screening in molecular SiH$_4$ [4]. This approach is also used to examine dynamical effects in biological organic materials such as photoactive yellow protein and dicyanovinyl-substituted oligothiophenes [37–39]. While it provides an efficient way to incorporate dynamical screening for a small number of excitonic states, e.g., around the absorption edge, it is not directly applicable for simulations of optical spectra, where a large number of excitonic states across a certain energy range is required. In addition, this approach approximates the true excitonic wave function by the static one, which is only valid when dynamical effects are small.

In this work, we follow Refs. [18,40] in using the Shindo approximation and a plasmon pole model for the analytical integration of the frequency-dependent dielectric function to obtain an expression for a single frequency-dependent dynamical BSE. We then implement and compare different approximations to numerically solve the dynamical BSE, including a static model with effective screening [30], the above-mentioned first-order perturbation approach [4], and exact diagonalization of the Hamiltonian. By solving the dynamical BSE directly on a frequency grid, we were able to examine not only the effect of dynamical screening on exciton-binding energies, but also on optical spectra. Our results show that while approximate treatments provide reasonable estimates of the magnitude of spectral shifts due to screening dynamics close to the absorption onset, small qualitative differences remain compared to the exact solution for excitonic states higher in energy. In addition, we show that an *effective* static screening, derived within the dynamical screening framework [30,41], requires only the lowest exciton-binding energy as input and still provides a good description of spectra. It provides a computationally tractable alternative, e.g., for studying complex or large numbers of materials.

In this work, we use crystalline naphthalene as an example. For this material, previous theoretical calculations report exciton binding energies of 0.9 eV, underestimating experimental measurements of 1.0–1.5 eV [33]. Since this exciton binding energy is about 10% of the plasma frequency, dynamical electronic screening can become important [4,18,30,37]. Our work provides a quantitative understanding of the importance of dynamical electronic screening and provides guidance for appropriate regimes of using different approximations when studying optical and excitonic properties of more complicated materials.

II. THEORETICAL APPROACH

The theoretical description of excitonic effects in this work starts from the Bethe-Salpeter equation (BSE) for the macroscopic (M) optical polarization function P^M. It follows from Hedin's equations for interacting electrons [42] and describes the probability amplitude of the process of annihilating an electron at $(\mathbf{r}'_2, t'_2)$ after creating one at $(\mathbf{r}'_1, t'_1)$, together with annihilating a hole at $(\mathbf{r_2}, t_2)$ after creating one at $(\mathbf{r_1}, t_1)$. In reciprocal and frequency space, the full BSE reads [18]

$$P^M(\lambda_1\lambda'_1, \lambda_2\lambda'_2, z_nz_m) = -i\hbar G_{\lambda_1}(z_n)G_{\lambda'_1}(z_n - z_m)\times \left\{ \delta_{\lambda_1\lambda'_2}\delta_{\lambda'_1\lambda_2} \right.$$
$$+ \frac{1}{-i\hbar\beta}\sum_{n'}\sum_{\lambda_3\lambda_4}\left[-W^{\lambda_1\lambda_3}_{\lambda'_1\lambda_4}(z_n - z_{n'}) \right.$$
$$\left. + 2\bar{v}^{\lambda_1\lambda'_1}_{\lambda_3\lambda_4} \right] \times P^M(\lambda_3\lambda_4, \lambda_2\lambda'_2, z_{n'}z_m) \left. \right\}.$$
$$(1)$$

Here, $\beta = 1/(k_{\mathrm{B}}T)$ where k_{B} is the Boltzmann constant and T is temperature. z_n and $z_{n'}$ are Fermionic Matsubara frequencies, corresponding to the Fourier components of the time difference between t_1 and t'_1, z_m is the bosonic Matsubara frequency, corresponding to the Fourier component of the time difference between t_1 and t_2. λ are indices for all single-particle electronic states. $G_\lambda(z) = 1/(\hbar z - E_\lambda)$ are single-particle Green's functions [4,43] with E_λ being the energy of the single-particle electron and hole state λ. W and $\bar{v}$ are the screened and the short-range bare Coulomb interaction of electrons and holes, respectively. It can be seen that the polarization function in Eq. (1) depends on *two* frequency arguments, z_n and z_m.

To describe optical excitation due to absorption of a single photon, one needs to obtain the polarization function that depends on only *one* frequency. In principle, this can be obtained by summing Eq. (1) over n [18],

$$P^M(\lambda_1\lambda'_1, \lambda_2\lambda'_2, z_m) = \frac{1}{-i\hbar\beta}\sum_n P^M(\lambda_1\lambda'_1, \lambda_2\lambda'_2, z_nz_m). \quad (2)$$

In practice, evaluating Eq. (2) is difficult for two reasons: First, to obtain each polarization function on the right-hand side, a complicated matrix problem needs to be solved that involves the n'-sum over the frequency-dependent screened Coulomb interaction in Eq. (1). Second, this procedure needs to be done many times for different z_n in order to evaluate the sum in Eq. (2).

A. Static Bethe-Salpeter equation

The standard approach to avoiding these difficulties is to neglect the frequency dependence of the screening, i.e., assuming

$$W(z_n - z_{n'}) \equiv W(0), \tag{3}$$

where $W(0)$ is the zero-frequency, static limit. It can be shown that with this approximation one can insert Eq. (1) into Eq. (2) and obtain a problem that only involves the polarization function that depends on a single frequency argument [4,18,43]

$$
P^M(\lambda_1 \lambda_1', \lambda_2 \lambda_2', z_m) = \frac{f(\lambda_1) - f(\lambda_1')}{E_{\lambda_1} - E_{\lambda_1'} - \hbar z_m} \times \left\{ \delta_{\lambda_1 \lambda_2'} \delta_{\lambda_1' \lambda_2} \right.
$$
$$
+ \sum_{\lambda_3 \lambda_4} \left[-W_{\lambda_1' \lambda_4}^{\lambda_1 \lambda_3} + 2\bar{v}_{\lambda_3 \lambda_4}^{\lambda_1 \lambda_1'} \right]
$$
$$
\left. \times P^M(\lambda_3 \lambda_4, \lambda_2 \lambda_2', z_m) \right\}. \tag{4}
$$

The Green's functions in Eq. (1) result in the term $\frac{f(\lambda_1) - f(\lambda_1')}{E_{\lambda_1} - E_{\lambda_1'} - \hbar z_m}$, where $f(\lambda)$ is the occupation factor of state λ. The crucial difference to Eq. (1) is that Eq. (4) contains only one frequency argument z_m and the complicated sum over n in Eq. (2) is avoided. Subsequently, Eq. (4) is transformed into a generalized eigenvalue problem [44].

From now on, we consider translational invariance, fully occupied valence states, and entirely empty conduction states, as is the case in semiconductor crystals at low temperature. This turns $\lambda \to c\mathbf{k}, v\mathbf{k}$, and the standard BSE Hamiltonian is obtained [4,18,44] as

$$\hat{H}_{vc\mathbf{k},v'c'\mathbf{k}'} = (E_{c\mathbf{k}} - E_{v\mathbf{k}})\delta_{vv'}\delta_{cc'}\delta_{\mathbf{k}\mathbf{k}'} + 2\bar{v}_{vc\mathbf{k}}^{v'c'\mathbf{k}'} - W_{vc\mathbf{k}}^{v'c'\mathbf{k}'}, \tag{5}$$

where $E_{c\mathbf{k}}$ and $E_{v\mathbf{k}}$ are the energies of the electronic state at point $\mathbf{k}$ in reciprocal space, and c and v represent conduction and valence band index, respectively. The term $\bar{v}_{vc\mathbf{k}}^{v'c'\mathbf{k}'}$

describes the bare Coulomb interaction, which is a short-range exchange term, and $W_{vc\mathbf{k}}^{v'c'\mathbf{k}'}$ describes the screened electron-hole Coulomb interaction that in the static approximation is computed using the inverse $\mathbf{q}$-dependent dielectric matrix $\varepsilon^{-1}(\mathbf{q}, \omega = 0)$. Solving the eigenvalue problem for the Hamiltonian in Eq. (5) provides pair resonance energies E_Λ and eigenfunctions $\mathbf{A}_\Lambda$ for excitonic states indexed by Λ. These are used to compute the dielectric function that can be compared to experiment, and to analyze exciton binding energies. The connection of the polarization function [$P(\omega)$] from the solution of the eigenvalue problem, and the dielectric function, is identical in the static and dynamical screening case, [$\varepsilon(\omega) = 1 - vP(\omega)$], see Ref. [18] for details.

B. Dynamical Bethe-Salpeter equation

To preserve the frequency dependence of W, an alternative way of obtaining a single-frequency dependent polarization function is through Shindo's approximation [36]. Instead of Eq. (3), this approximation expresses the two-frequency dependent polarization function $P^M(z_n z_m)$ in Eq. (1) directly in terms of the Green's function of noninteracting electrons and holes and the one-frequency dependent polarization function $P^M(z_m)$, see Eq. (S1) in the supplemental information [45]. This approximation leads to an expression for the single-frequency dependent polarization function that takes a very similar form as Eq. (4), with the frequency-independent screened Coulomb interaction W replaced by an effective, frequency-dependent $\tilde{W}(z_m)$ [18] (see Eq. (S3) in Ref. [45]). Considering only real frequencies involved in optical excitations ($z_m \to \omega$) allows the transformation into an eigenvalue problem for the frequency-dependent BSE Hamiltonian [18]

$$\tilde{H}_{vc\mathbf{k},v'c'\mathbf{k}'}(\omega) = (E_{c\mathbf{k}} - E_{v\mathbf{k}})\delta_{vv'}\delta_{cc'}\delta_{\mathbf{k}\mathbf{k}'} + 2\bar{v}_{vc\mathbf{k}}^{v'c'\mathbf{k}'} - \tilde{W}_{vc\mathbf{k}}^{v'c'\mathbf{k}'}(\omega). \tag{6}$$

Compared to Eq. (5), the frequency dependence of Eq. (6) comes from the effective, frequency-dependent screened Coulomb interaction $\tilde{W}(\omega)$ which takes the form [4,18]

$$
\tilde{W}_{vc\mathbf{k}}^{v'c'\mathbf{k}'}(\omega) = \frac{1}{V} \sum_{\mathbf{q},\mathbf{G},\mathbf{G}'} v(\sqrt{|\mathbf{q}+\mathbf{G}||\mathbf{q}+\mathbf{G}'|}) B_{cc',\mathbf{k}\mathbf{k}'}(\mathbf{q}+\mathbf{G}) B_{vv',\mathbf{k}\mathbf{k}'}^*(\mathbf{q}+\mathbf{G}') \left\{ \delta_{\mathbf{G}\mathbf{G}'} + \int_0^\infty \frac{d\hbar\omega'}{\pi} \mathrm{Im}\,\varepsilon^{-1}(\mathbf{q}+\mathbf{G}, \mathbf{q}+\mathbf{G}', \omega') \right.
$$
$$
\left. \times \left[\frac{1}{\hbar\omega' + E_{c\mathbf{k}} - E_{v'\mathbf{k}'} - \hbar\omega} + \frac{1}{\hbar\omega' + E_{c'\mathbf{k}'} - E_{v\mathbf{k}} - \hbar\omega} \right] \right\} \delta_{\mathbf{q},\mathbf{k}-\mathbf{k}'}, \tag{7}
$$

where v is the Coulomb potential in reciprocal space. In addition, V is the volume of the unit cell, $\mathbf{q}$ represents the reciprocal wave vector, $\mathbf{G}$ and $\mathbf{G}'$ are reciprocal lattice vectors. $\varepsilon(\mathbf{q}+\mathbf{G}, \mathbf{q}+\mathbf{G}', \omega')$ is the frequency and wave-vector dependent dielectric function. The terms $B_{cc',\mathbf{k}\mathbf{k}'}$ and $B_{vv',\mathbf{k}\mathbf{k}'}$ are the Bloch integrals that account for the overlap between single particle Bloch wave functions [18]:

$$B_{cc',\mathbf{k}\mathbf{k}'}(\mathbf{q}+\mathbf{G}) = \delta_{\mathbf{q},\mathbf{k}-\mathbf{k}'}\langle u_{c\mathbf{k}}|e^{i\mathbf{G}\cdot\mathbf{r}}|u_{c'\mathbf{k}'}\rangle, \tag{8}$$

where $u_{c\mathbf{k}}(r)$ represents the Bloch-periodic part of the Kohn-Sham state $\psi_{c\mathbf{k}}$. The frequency integral in the second term

inside the curly brackets results from Shindo's approximation [18], since the two-frequency dependence is replaced by a sum over single-frequency dependent polarization functions [18,36]. We note that the Shindo approximation uses the screened Coulomb interaction W, that is also part of the GW approximation, and turns it into $\tilde{W}$ via Eq. (S4) of Ref. [45]. $\tilde{W}$ is more complicated due to the additional energy denominator terms.

We refer to the supplemental information Eq. (S3) for the single frequency dependent polarization function using Shindo's approximation [45] and Ref. [18] for the derivation

of Eq. (7), as well as for complete details on how to obtain the eigenvalue problem from the BSE, which is identical in the static and dynamic case. The form of the frequency dependent screened Coulomb potential Eq. (7) has also been derived in multiple other references [4,36,46]. Shindo's approximation is argued to be a first-order approximation with respect to the dynamical nature of the screened potential [18,47–50]. Without assuming static screening in the BSE, the Shindo approximation, Eq. (S1), requires a small difference of the dynamic potential and an effective static potential. It uses only the zeroth order of an expansion in the difference of these two potentials, leading to Eqs. (S3) and (S4). We show later in Secs. IV B and IV C that in our work, this requirement is fulfilled since the dependence of the excitation energy on frequency is an order of magnitude smaller than the excitation energy itself. We will show that the dynamical correction does not exceed 15% of the exciton binding energy. However, studying its validity quantitatively is very hard and has not been accomplished so far. In this work, we analyze dynamical screening effects within the framework of Shindo's approximation, and do not consider any effects beyond.

With Eqs. (6) and (7), two aspects need to be addressed to solve the dynamical problem. First, an eigenvalue problem needs to be solved similar to the static case, however, now with a frequency-dependent BSE Hamiltonian. Second, one needs to evaluate the frequency-dependent screened Coulomb interaction, Eq. (7). In the following, we discuss practical ways to address the first aspect in Sec. II C and the second aspect in Sec. II D.

C. Dynamical eigenvalue problem

A dynamical eigenvalue problem needs to be solved for the frequency-dependent BSE Hamiltonian in Eq. (6),

$$\tilde{H}(\omega)\mathbf{A}_\Lambda(\omega) = E_\Lambda(\omega)\mathbf{A}_\Lambda(\omega), \qquad (9)$$

to obtain the frequency-dependent excitonic eigenvalues and eigenfunctions. Different from the static case, where this set of solutions directly provides excitation energies, in the case of dynamical screening, one needs to find the solution of [18]

$$E_\Lambda(\omega) = \hbar\omega. \qquad (10)$$

Physically, this represents the condition where the energy of excitonic state Λ equals the energy of the absorbed photon and it amounts to identifying the state Λ that was computed using the corresponding photon frequency. In the following, we discuss three different approaches to accomplish this: Exact diagonalization of the dynamical Hamiltonian, a perturbative treatment of the problem [4], and an *effective* static screening approximation [30,41].

In the exact diagonalization approach, the excitation energy $E_\Lambda(\omega)$ can be obtained by sampling the frequency ω on a grid and solving one eigenvalue problem at each frequency point. Subsequently, Eq. (10) can be solved via interpolation of this data or using the nearest data point on the frequency grid that minimizes $E_\Lambda(\omega) - \hbar\omega$. Compared to the static BSE, this increases the complexity by at least a factor of N, where N is the number of frequency sampling points. We note that this computational cost can be somewhat mitigated using efficient solvers of eigenvalue problems, such as the ChASE library

[51], that we recently interfaced with our BSE code [52], demonstrating speedups on the order of a factor of five in solving the static BSE.

The perturbative approach to solving Eq. (10) was proposed by Rohlfing and Louie [4]. It treats the dynamical effect of the screened Coulomb potential as a first-order perturbation to the solutions of the static BSE. The solutions E_Λ^{sta} of the static eigenvalue problem for each excitonic state Λ are used as the input frequency $\hbar\omega$ in Eq. (7) to the dynamical screening function $\tilde{W}(\omega)$. Next, the difference between the resulting approximated dynamical screening potential and the static screening potential $\tilde{W}(E_\Lambda^{\text{sta}}) - W^{\text{sta}}$ is treated as a first-order perturbation, so that the solution for each state Λ becomes

$$E_\Lambda^{\text{dyn}} \approx E_\Lambda^{\text{sta}} + \langle A_\Lambda | \tilde{W}(E_\Lambda^{\text{sta}}) - W^{\text{sta}} | A_\Lambda \rangle, \qquad (11)$$

where $|A_\Lambda\rangle$ are the eigenfunctions of the static BSE Hamiltonian (5).

Validity of the perturbative treatment requires two conditions: (1) E_Λ^{sta} is reasonably close to the true solution such that evaluating $\tilde{W}(\omega)$ at $\hbar\omega = E_\Lambda^{\text{sta}}$ is close to the true dynamical screening function for each state Λ, and (2) the difference $\tilde{W}(E_\Lambda^{\text{sta}}) - W^{\text{sta}}$ is small, so that dynamical effects can be considered as a first-order perturbation. Reference [4] recommends to iterate several times and reports quick convergence, and, indeed, we verified that the solution converges within two to three steps. Instead of solving the entire problem on a frequency grid, this approach focuses on a few specific excitonic states and only updates the energy of those states based on the static solutions, leaving the excitonic wave functions unchanged. This provides a fast route to solving the dynamical problem especially when only a few excitonic states, e.g., the lowest ones, are of interest. However, its validity needs to be examined for systems where dynamical effects are significant, since in this case, the solutions obtained through the static approximation can differ significantly from the dynamic ones.

As can be seen in Eq. (11), the perturbative approach requires evaluating the screened interaction $\tilde{W}(E_\Lambda^{\text{sta}})$ for each state Λ of interest. This is not practical for simulations of spectra, where a large number of eigenstates N_Λ is required. In this work, we instead group the E_Λ^{sta} into energy intervals of 0.3 eV which allows us to reduce the number of times we need to evaluate the screening matrix $\tilde{W}(E_\Lambda^{\text{sta}})$ from N_Λ to the number of chosen frequency intervals. For eigenstate Λ with an eigenvalue E_Λ^{sta} in a given interval, the dynamical screening function is approximated by the lower end of the interval. In Sec. IV of this work, the number of screening potential evaluations needed to compute dynamical corrections to the energies and spectra is reduced from 10^4 to about 30.

In addition, we note that in practice even for static screening the full diagonalization is usually avoided, using, e.g., a time propagation approach [53,54]. This would be feasible in the context of this work only when using the effective static approach discussed in the following. In this approach, effective, static screening can be adopted to obtain an approximate solution of Eq. (10). This bypasses the frequency-dependent eigenvalue problem entirely but instead focuses on approximating Eq. (7) by replacing the energy difference terms $E_{c'\mathbf{k}'} - E_{v\mathbf{k}} - \hbar\omega$ and $E_{c\mathbf{k}} - E_{v'\mathbf{k}'} - \hbar\omega$ by an effective,

constant exciton-binding energy, which is independent of the energies of the electronic states and $\hbar\omega$. This reduces the dynamical screening problem to an effectively static problem since the two terms in the brackets of Eq. (7) reduce to one single value, that can be chosen as the binding energy of the lowest excitonic state

$$E_b = E_g - E_{\Lambda=0}^{\text{sta}}, \tag{12}$$

where E_g is the band gap without considering excitonic effects. As a result, this approach replaces the dynamical screening function with an effective static screening function, that takes the exciton binding energy of the material explicitly into consideration and Eq. (7) is simplified to [30]

$$\tilde{W}_{cc',vv',\mathbf{kk}'}^{\text{eff}} = \frac{1}{V} \sum_{\mathbf{q,G,G}'} v(\sqrt{|\mathbf{q+G}||\mathbf{q+G}'|}) B_{cc',\mathbf{kk}'}(\mathbf{q+G})$$

$$\times B_{vv',\mathbf{kk}'}^*(\mathbf{q+G}') \left\{ \delta_{\mathbf{GG}'} + \int_0^\infty \frac{d\hbar\omega'}{\pi} \right.$$

$$\times \left. \text{Im}\varepsilon^{-1}(\mathbf{q+G, q+G}', \omega') \frac{2}{\hbar\omega' + E_b} \right\} \delta_{\mathbf{q,k-k}'}. \tag{13}$$

The resulting Eq. (13) contains no frequency dependence anymore since ω' can be integrated explicitly. This approach is the cheapest among the three, as it is a modified version of the static approximation and it has been used to study effects of free-carrier screening [30] and the screening of lattice polarizability [41]. In addition, among the three approaches we introduced, the effective static screening does not require the excitonic wave function, allowing us to take advantage of the time propagation approach [53,54] to avoid the diagonalization of the eigenvalue problem. In Ref. [30], the authors argue that the process can be repeated several times to converge the solution. However, we note that it needs to be tested whether the converged values will match the true solution of the frequency-dependent BSE.

D. The dynamical screening function

In order to proceed with solving the dynamical eigenvalue problem, Eq. (9), one needs to compute the *frequency-dependent* screened Coulomb interaction, Eq. (7). The major challenge lies in the frequency integral with respect to ω'. While it can be evaluated numerically, e.g., within the random-phase approximation [19,55], this comes with high computational cost, since one ω' integral needs to be evaluated

explicitly for each ω and each combination of $cv\mathbf{k}$ and $c'v'\mathbf{k}'$, see Eq. (7).

The integral can be carried out explicitly if an analytical model function is assumed for the ω' dependence of the inverse dielectric matrix. In this work, we pursue that route and use the generalized plasmon-pole approximation (PPA) from Hybertsen and Louie [4,40,56] to carry out the frequency integral. This model expresses the frequency dependent inverse dielectric matrix to be a pole function of the form

$$\text{Im}\,\varepsilon^{-1}(\mathbf{q+G, q+G}', \omega) = A(\mathbf{q+G, q+G}')$$

$$\times \{ \delta[\omega - \tilde{\omega}(\mathbf{q+G, q+G}')]$$

$$- \delta[\omega + \tilde{\omega}(\mathbf{q+G, q+G}')] \}, \tag{14}$$

$$\text{Re}\,\varepsilon^{-1}(\mathbf{q+G, q+G}', \omega) = 1 + \frac{\Omega^2(\mathbf{q+G, q+G}')}{\omega^2 - \tilde{\omega}^2(\mathbf{q+G, q+G}')}. \tag{15}$$

The three parameters $A(\mathbf{q+G, q+G}')$, $\tilde{\omega}(\mathbf{q+G, q+G}')$, and $\Omega(\mathbf{q+G, q+G}')$ are given by the following additional constraints: the Kramers-Kronig relation, the f-sum rule, and the *static* inverse dielectric matrix $\varepsilon^{-1}(\mathbf{q+G, q+G}', \omega=0)$ [40]. To describe the wave-vector dependence of the *static* inverse dielectric matrix we adopt the model from Bechstedt *et al.* [57], which considers only diagonal terms $\mathbf{G = G}'$. It interpolates between free-electron gas behavior at large $\mathbf{q}$ and Thomas-Fermi like behavior at small $\mathbf{q}$ [44,57,58]. The approximation of neglecting local-field effects in the screening ($\mathbf{G = G}'$) is reasonable in typical semiconductors [20,57,59]. Whether it can impose problems for studying dynamical screening effects, e.g., when excitons become more localized, remains worthwhile exploring in the future.

With the above constraints the three parameters of the plasmon-pole model follow as (see the supplemental information section B for details of the derivation [45])

$$\Omega(\mathbf{q+G}) = \omega_p, \tag{16}$$

$$\tilde{\omega}(\mathbf{q+G}) = \omega_p[1 - \varepsilon^{-1}(\mathbf{q+G}, \omega=0)]^{-1/2}, \tag{17}$$

$$A(\mathbf{q+G}) = -\frac{\pi}{2}\omega_p[1 - \varepsilon^{-1}(\mathbf{q+G}, \omega=0)]^{1/2}. \tag{18}$$

Carrying out the frequency integral in Eq. (7) then provides the dynamical screening potential

$$\tilde{W}_{cc',vv',\mathbf{kk}'}(\omega) = \frac{1}{V} \sum_{\mathbf{q,G}} v(|\mathbf{q+G}|) B_{cc',\mathbf{kk}'}(\mathbf{q+G}) B_{vv',\mathbf{kk}'}^*(\mathbf{q+G}) \left\{ 1 - \frac{\hbar\omega_p}{2}[1 - \varepsilon^{-1}(\mathbf{q+G}, \omega=0)]^{1/2} \right.$$

$$\times \left[\frac{1}{\hbar\omega_p(1 - \varepsilon^{-1}(\mathbf{q+G}, \omega=0))^{-1/2} + E_{c\mathbf{k}} - E_{v'\mathbf{k}'} - \hbar\omega} \right.$$

$$+ \left. \left. \frac{1}{\hbar\omega_p(1 - \varepsilon^{-1}(\mathbf{q+G}, \omega=0))^{-1/2} + E_{c'\mathbf{k}'} - E_{v\mathbf{k}} - \hbar\omega} \right] \right\} \delta_{\mathbf{q,k-k}'}. \tag{19}$$

In the effective static screening approach, the energy differences in the denominator are replaced by the exciton binding energy, see Eq. (12), resulting in

$$\tilde{W}^{\text{eff}}_{cc',vv',\mathbf{kk'}} = \frac{1}{V} \sum_{\mathbf{q},\mathbf{G}} v(|\mathbf{q}+\mathbf{G}|) B_{cc',\mathbf{kk'}}(\mathbf{q}+\mathbf{G}) B^*_{vv',\mathbf{kk'}}(\mathbf{q}+\mathbf{G})$$

$$\times \left\{ 1 - \frac{\hbar\omega_p}{2}[1-\varepsilon^{-1}(\mathbf{q}+\mathbf{G},\omega=0)]^{1/2} \left[\frac{2}{\hbar\omega_p(1-\varepsilon^{-1}(\mathbf{q}+\mathbf{G},\omega=0))^{-1/2}+E_b} \right] \right\} \delta_{\mathbf{q},\mathbf{k}-\mathbf{k'}}. \qquad (20)$$

The denominators in Eqs. (19) and (20) significantly determine the nature of screening through the interplay between the plasma frequency ω_p as a characteristic frequency, and exciton binding, either expressed as the two energy differences $E_{c'\mathbf{k'}} - E_{v\mathbf{k}} - \hbar\omega$ and $E_{c\mathbf{k}} - E_{v'\mathbf{k'}} - \hbar\omega$ in Eq. (19) or E_b in Eq. (20). The static limit corresponds to negligible exciton binding compared to the plasma frequency and can be obtained from Eqs. (19) and (20) by dropping these energy differences or E_b, respectively. In this case, all terms in the curly brackets reduce to $\varepsilon^{-1}(\mathbf{q}+\mathbf{G},\omega=0)$. In bulk semiconductors, plasma frequencies are usually several eV to several tens of eV and exciton-binding energies are several tens to a few hundreds of meV, i.e., at least one order of magnitude smaller, illustrating the validity of the static approximation. In many low-dimensional or organic semiconductors, however, the exciton binding energies are relatively large and can be on the order of 1 eV [33,60,61], rendering the validity of the static approximation questionable. Furthermore, this illustrates, e.g., for the lowest bound excitonic state, that including electronic screening dynamics effectively reduces screening compared to the static approximation, leading to stronger excitonic effects. This is because the denominator of Eq. (19) is larger than when E_b is dropped in the static case. Hence, dynamical screening is effectively weaker and in the static approximation screening is always overestimated. Physically, this can be interpreted as an initially incomplete screening in the dynamic case, compared to an instantly formed screening in the static approximation [18].

III. COMPUTATIONAL METHODS

In this work, we compare the three different approaches to describe screening dynamics, i.e., exact diagonalization, perturbative treatment, and the effective static screening approach, for optical spectra and exciton binding energies of crystalline naphthalene. This material is an organic crystal for which large exciton binding energies of 1.0–1.5 eV were reported from experiment [33]. We implemented the three different approaches using the plasmon-pole approximation (PPA), into the BSE implementation discussed in Refs. [44,58], based on the Vienna *ab initio* simulation package [62–64] (VASP).

For naphthalene, we first performed density functional theory [11,12] (DFT) simulations using the generalized-gradient approximation (GGA) by Perdew, Burke, and Ernzerhof (PBE) to describe exchange and correlation [65] and the projector-augmented wave (PAW) scheme [66] to model the electron-ion interaction. Kohn-Sham states were expanded into plane waves up to a cutoff energy of 400 eV. We used

lattice constants that were reported from experiment [67] and relaxed atomic positions until all Hellmann-Feynman forces were smaller than 5 meV/Å, using the DFT-D2 method of Grimme [68] to capture Van der Waals corrections. For these relaxations, the Brillouin zone (BZ) was sampled using $3\times5\times3$ Γ-centered $\mathbf{k}$ points. We verified that the total energy of the unit cell is converged to better than 1 meV/atom with these parameters.

For the BSE simulations, we computed the DFT-PBE electronic structure for the relaxed atomic geometries described above and tested convergence with respect to BZ sampling and BSE cutoff energy, i.e., the energy up to which noninteracting electron-hole pairs are included in the BSE Hamiltonian. We did these tests using static screening and all details can be found in Ref. [45] (see Figs. S4–S6). We find that, contrary to materials with dispersive valence and conduction bands such as MgO and ZnO [44,69], the valence and conduction band edges of naphthalene are flat (see Fig. S1) and the exciton binding energy of naphthalene converges quickly with BZ sampling (see Fig. S5). We obtain the value of the exciton binding energy by extrapolating to infinitely dense sampling as discussed in Ref. [44]. Balancing computational cost and accuracy of the BSE calculations of optical spectra, we adopted a $5\times7\times5$ $\mathbf{k}$-point grid centered at the A point of the BZ, to capture the lowest-energy transitions near that point. We use a BSE cutoff energy of 14 eV to compute spectra with static screening and compare these to literature results in Fig. 2. Due to the larger computational cost of dynamical screening, we reduce the BSE cutoff energy to 9 eV for investigating dynamical effects, and focus on the spectra between the onset at 3 eV and up to 5.5 eV. Based on the convergence tests above, we anticipate that the choice of the energy cutoff and $\mathbf{k}$-point sampling results in deviations of about 0.2 eV compared to the converged values, however, we show in Sec. G of Ref. [45] that the error induces constant shifts to the predicted exciton binding energy, and we do not expect them to affect our analysis of dynamical screening effects. In all spectra calculations, a Lorentzian life-time broadening of 0.1 eV is used. In the static model dielectric function, a high-frequency dielectric constant of 2.35 is used, and is chosen based on the experimental value [70,71].

IV. RESULTS AND DISCUSSION

We compute the optical spectra and exciton binding energies of the organic crystal naphthalene using static screening in the BSE and the three different approaches to dynamical electronic screening discussed above. The unit cell of naphthalene is shown in Fig. 1 and consists of two units of
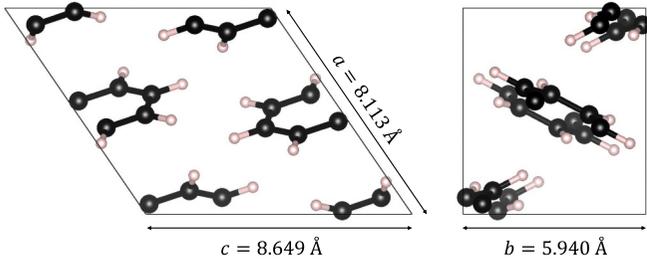
FIG. 1. Monoclinic naphthalene ($C_{10}H_8$) viewed from the crystalline *b* direction (left) and the crystalline *c* direction (right). Black spheres represent carbon atoms and white spheres represent hydrogen atoms. The unit cell consists of two conjugated orientated naphthyl rings. The crystal structure is obtained from Ref. [67] and we subsequently fully relaxed all atomic positions.

double carbon rings with conjugated orientation. This system is an ideal test bed to systematically study dynamical effects in the description of electronic screening, since it exhibits exciton binding energies on the order of 1 eV [33,72,73], which is an order of magnitude larger than exciton binding energies of typical bulk inorganic semiconductors of several 10 meV [74–76]. Using the independent-particle approach in VASP and the integral from the f-sum rule without considering the electron-hole interaction, we compute a plasma frequency of 17.9 eV, which is similar to bulk inorganic materials. The closer the exciton binding energy is to the plasma frequency, the more important are dynamical effects for electronic screening, and this is what we expect for naphthalene in this work.

A. Independent quasiparticle approximation and static BSE

We first compute the optical spectrum of naphthalene using the independent-quasiparticle approximation within the GGA + Δ approach as well as the static BSE, see Fig. 2. In
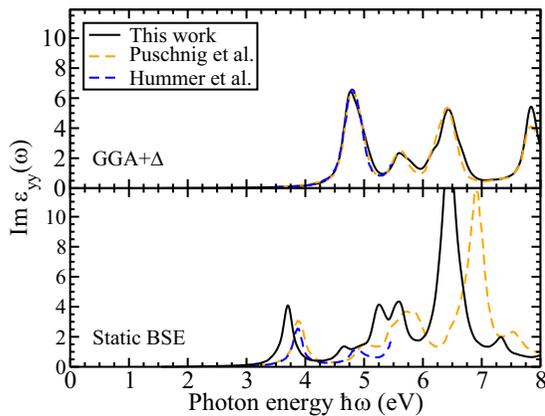

FIG. 2. Imaginary part of the $\varepsilon_{yy} \parallel b$ component of the dielectric tensor, calculated without electron-hole interaction (top) and from solving the BSE with statically screened electron-hole interaction (bottom). We used the high-frequency dielectric constant from experiment [70,71], $\varepsilon_\infty = 2.35$, and a scissor shift of $\Delta = 1.55$ eV. The shape of our spectra agrees very well with data by Puschnig *et al.* [77] and Hummer *et al.* [33].

this work, we focus on optical spectra and exciton binding energy for the *y* polarization, i.e., the ε_{yy} component of the dielectric tensor parallel to the crystalline *b* direction, since for this direction the lowest-energy excitonic eigenstates were reported [33,72]. Our calculated value for the GGA band gap, $E_g^{GGA} = 3.12$ eV, agrees well with an earlier result of 3.10 eV [72]. We use a scissor shift of $\Delta = 1.55$ eV so that the first bright peak is at the same position at 4.8 eV as reported from quasiparticle calculations [33]. Details of the band structure can be found in Fig. S1 of Ref. [45]. The upper panel of Fig. 2 shows good agreement between our GGA + Δ result and a spectrum from the literature [33,77]. We notice that some differences are observed at the peak around 8 eV, as the height of the peak from our calculation is slightly larger. We also verified that our results agree very well with a GGA + Δ spectrum using a broadening of 0.05 eV [72], if we adopt the same broadening (see Ref. [45] Sec. D).

When including the electron-hole interaction by solving a BSE with static screening, we find strong excitonic effects in naphthalene and indeed report an exciton-binding energy of 1.06 eV. The difference between the first main peak with (BSE) and without (GGA + Δ) excitonic effects, see upper and lower panel of Fig. 2, is used to obtain the value of the exciton binding energy, similar as in Ref. [33]. Comparing our static BSE spectrum with earlier results in the literature in the lower panel of Fig. 2 shows reasonable agreement also of the overall spectral shape [33,77]. We note that Puschnig *et al.* used a broadening of 0.2 eV [77], possibly explaining some of the deviations with respect to our data. In addition, our predicted exciton binding energy is slightly larger than 0.9 eV reported in Ref. [33], and correspondingly, the onset of our spectrum in Fig. 2 appears at slightly lower energy. We attribute this to the different approaches of describing the wave-vector dependence of the screening in the static BSE. While our work uses the Bechstedt model and the experimental high-frequency dielectric constant of 2.35 [70,71], Refs. [33,77] use the RPA based on the Kohn-Sham eigenvalues [78], and the corresponding dielectric constant computed within the independent particle approximation is reported in Ref. [77] as 3.8.

B. Dynamical electronic screening

We now compare the spectra we computed from solutions of the BSE that account for electronic screening dynamics via the three different approaches discussed in Sec. II. First, we compute excitonic eigenvalues E_Λ via direct diagonalization by sampling a frequency grid to solve Eq. (10). Figure 3 shows this sampling of the frequency range of interest with a spacing of 0.3 eV and our computed solutions for the excitonic eigenvalues E_Λ. This figure shows that there is no complicated dependence on frequency, illustrating that a simple interpolation scheme is appropriate and our frequency spacing of 0.3 eV is sufficient. We further verified this by calculating spectra using different samplings, and the results can be found in Fig. S3 of Ref. [45]. Here we use a nearest neighbor approximation, i.e., for each state, the solution that is the closest to the $E_\Lambda(\omega) = \hbar\omega$ line is adopted as the solution of the dynamical problem for that state. This allows us to also compute optical spectra, which requires excitonic wave
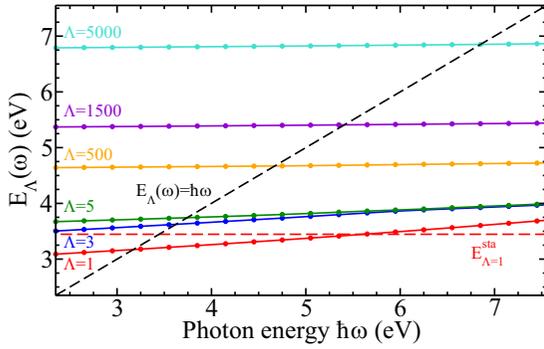
FIG. 3. Frequency dependent exciton eigenvalues $E_\Lambda(\omega)$ for excitonic states Λ, obtained using exact diagonalization of the Hamiltonian in Eq. (9). We show various randomly selected states to cover a range of exciton energies. We find the solution of $E_\Lambda(\omega) = \hbar\omega$ (black dashed line) via a nearest neighbor approximation (see text). The solution using the standard static approximation for the lowest excitonic state ($\Lambda = 1$) is marked with the horizontal red-dashed line.

functions that would be more challenging to obtain in an interpolation scheme. We estimate from Fig. 3 that the nearest neighbor approximation does not cause an error in the solution of more than 0.01 eV. Nevertheless, Fig. 3 illustrates, e.g., for the $\Lambda = 1$ state, that an exciton binding energy of 1.49 eV compared to the plasma frequency of 17.9 eV is affected by the frequency dependence due to electronic screening dynamics.

In the upper two panels of Fig. 4, we compare the optical spectra from the exact diagonalization of the dynamical
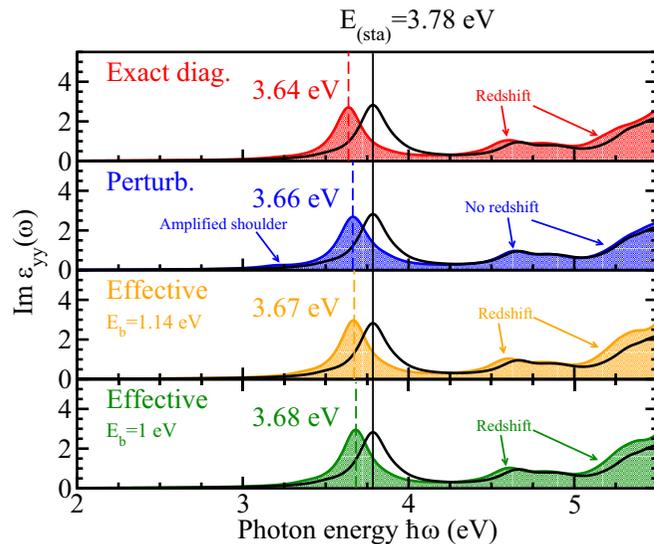

FIG. 4. Comparison of ε_{yy} from the static BSE (black solid lines) with the different approaches to include dynamical screening. Red shows the exact diagonalization and blue results from the perturbative approach. Effective static screening using $E_b = 1.14$ eV (orange) and $E_b = 1$ eV (green) is also shown. All curves use a scissor shift of 1.55 eV. The positions of the first major peak are highlighted in the figure with vertical dashed lines. We also note that an excitonic state is visible when adopting the perturbative approach, that is dark in all other cases.

problem and the perturbative approach to our static BSE result. This comparison shows that the perturbative treatment works well for the lowest-energy major peak predicted by the static approximation at 3.78 eV, as it predicts a 0.12 eV redshift from the peak with static screening, compared to a redshift of 0.14 eV when the exact diagonalization approach is used. Figure 4 also shows a redshift of all spectra that include screening dynamics relative to the static case, which confirms the expected effective reduction of screening when dynamics is included, as discussed in Sec. II D.

Further comparison shows that the perturbative treatment results in a magnified excitonic shoulder at a photon energy of 3.25 eV, see Fig. 4, which neither of the other techniques shows. We find a corresponding excitonic eigenvalue using all three approximations to dynamical screening, however, its oscillator strength is much smaller in the case of exact diagonalization and for the effective static treatment of screening. Inclusion of screening dynamics reduces the oscillator strength of the underlying excitonic states. The perturbative approach struggles with this, as it uses unchanged excitonic eigenfunctions of the static simulation. In addition, at higher energies beyond about 4.2 eV, we see that the perturbative treatment strongly resembles the static result, while all other approaches yield an overall redshift and an enhancement of the shoulder near 5 eV (see Fig. 4).

Finally, we investigate the effective static screening approximation, see Eq. (20). In Fig. 4, we show results for effective static screening using the exciton-binding energy calculated from the static screening approximation (1.0 eV) and that from exact diagonalization (1.14 eV), leading to dynamical screening corrections of 0.10 and 0.11 eV, respectively. The lower two panels of Fig. 4 show that both cases underestimate the correction due to dynamical screening compared to the exact diagonalization. The position of the first peak is about 0.03–0.04 eV higher in energy, i.e., closer to the static approach, corresponding to a 28.5% and 21.4% change of the dynamical correction to the exciton binding energy when compared to exact diagonalization. Overall, however, effective static screening describes spectra better than the perturbative approach especially at higher energies as the perturbative treatment fails to capture the redshift due to dynamical effects qualitatively. As a result, we recommend the effective static approximation over the perturbative approach to include dynamical screening when optical spectra over a range of photon energies are considered.

We provide an analysis to understand the difference we observed above between the different approaches: including screening dynamics either via exact diagonalization or via the effective static screening approach changes how individual single-particle Kohn-Sham states are combined into excitonic wave functions. This is because the matrix elements of the BSE Hamiltonian change and the eigenstate of that Hamiltonian determines the exciton wave function. Such a change of single-particle KS contributions can affect how strongly or weakly a certain feature appears in the spectrum. In the case of the perturbative approach, see Eq. (11), the exciton wave functions themselves are kept constant and mixing of individual KS states is not changed, relative to static screening BSE simulations.

We note that Hummer *et al.* [33] report a minor underestimation of the exciton-binding energy compared to experiment. Their theoretical value is 0.9 eV, while experimental results are reported as 1.0–1.5 eV [33]. We find that the reduction of the screening due to dynamical effects provides an additional redshift to the spectra, putting the predicted exciton-binding energy closer to the range of the experimental values. This is additional evidence that electronic dynamical screening effects need to be taken into consideration for accurate modeling of these systems where large exciton-binding energies are observed. We note that while lowest singlet excitation energies reported from experiment are reasonably consistent (3.9–4.0 eV [79–82]), a variation of the reported electronic gap (5.0–5.4 eV [79,83–85]) is seen, due to the models used to extract the gap from photoemission experiments. This causes a variation of the estimated binding energy from experiments on the order of 0.5 eV. Even if we exclude the electronic band gap of 5.0 eV reported in Ref. [79] from observations of the change in carrier generation, the remaining references still show a variation of 5.1–5.4 eV with an error bar on the order of 0.2 eV due to uncertainty in empirical parameters [85], resulting in an estimated exciton-binding energy of 1.2–1.5 eV.

C. Influence of the plasmon-pole model

As discussed in Sec. II D, in this work a plasmon-pole model is adopted to derive Eq. (19), which requires the plasma frequency ω_p as an input to calculate the screened Coulomb potential. We compute $\omega_p = 17.9$ eV within independent-particle approximation, i.e., without considering the electron-hole interaction, through integrating the imaginary part of the dielectric function using the VASP code and averaging over the Cartesian coordinates. It has been found previously that the enforcement of the f-sum rule of the HL PPM model can overestimate the energy of the pole of the dielectric function, e.g., by about 10% for elemental carbon [86].

Hence, in the following we examine the influence of the plasmon-pole frequency ω_p on our results and varied ω_p in a ~10% range from the calculated value, between 16 and 19 eV, to examine the influence on resulting spectra and exciton-binding energy. From the spectra shown in Fig. 5 we see that with increasing plasma frequency from 16 to 19 eV, the first major peak is slightly blue shifted because the predicted red shift due to dynamical screening corrections is increased from 0.14 to 0.16 eV, i.e., by about 15%. This reduction of the dynamical correction is expected, since increasingly large ω_p corresponds more closely to the static screening case, as discussed in Sec. II D, reducing dynamical corrections and increasing the strength of dielectric screening. However, the influence is not substantial around the plasma frequency of interest in this work. Overall, we found that the potential overestimation of the pole energy due to the choice of the plasmon-pole model, does not qualitatively affect the significance of dynamical effects. We also note that the dependence on the plasmon-pole energy is similar to that of the effective static method and a similar trend is expected in this case.

Finally, we note that for naphthalene, the exciton binding energy is only 5% of the plasma frequency. However, the ratio
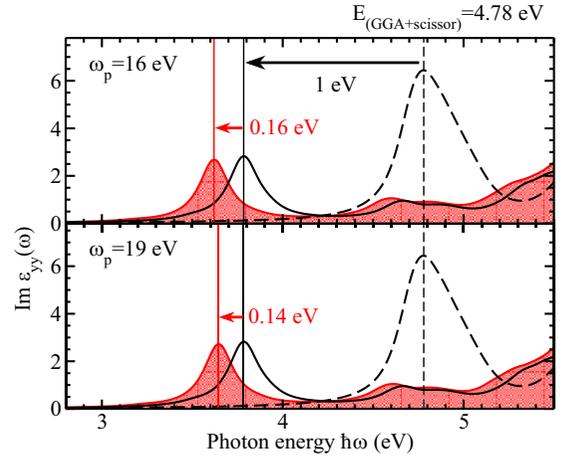

FIG. 5. Imaginary part of the $\varepsilon_{yy} \parallel b$ component of the dielectric tensor from static BSE (black solid line) and independent quasiparticle approximation (GGA+scissor, black dashed line) are compared to exact diagonalization results computed using different values of the plasmon frequency (red shaded). We show that increasing ω_p from 16 to 19 eV changes the prediction of the correction on the exciton binding energy due to dynamical screening effects from 0.16 to 0.14 eV.

between exciton binding energy and characteristic frequency that determines screening dynamics is much larger in other important applications of the BSE technique. For example, in the case of phonon screening in polar materials, the characteristic frequency scale to compare to is that of phonon frequencies, instead of the plasma frequency [41]. In this case, the exciton-binding energy is on the same order compared to the characteristic frequency, and screening dynamics is expected to be important for an accurate description of optical properties.

V. CONCLUSION

We examined the effects of electronic dynamical screening of the electron-hole interaction when solving the Bethe-Sapleter equation of the optical polarization function for a naphthalene organic crystal. By adopting the Shindo approximation and a plasmon-pole model, the BSE can be written as a frequency-dependent eigenvalue problem. We compared three different ways of addressing this dynamical problem, i.e., exact diagonaliztion of the frequency-dependent BSE Hamiltonian, perturbative treatment of the static eigenstates, and an effective static approximation. The exact-diagonalization approach requires solving the BSE Hamiltonian at numerous frequencies to obtain the eigenenergies and eigenstates. The perturbative approach requires diagonalization of the BSE Hamiltonian in the static approximation in order to obtain the excitonic wave functions. Meanwhile, the effective screening approach bears the same cost of the standard approach of solving the BSE within the static approximation.

We show that for naphthalene, all three methods induce a ~15% correction of the exciton binding energy, predicted to be around 1 eV by the standard static approximation. While the exact diagonalization constitutes a reference case in this work, it comes at high computational cost that renders this

approach unfeasible for computing spectra. The perturbative treatment is a decent alternative that does not require full solution of multiple BSE Hamiltonians while providing good qualitative estimates of binding energies of the lowest excitonic states. Finally, we show that for spectra, the effective static screening approach is well suited and numerically efficient, possible allowing application to complex materials. The results for naphthalene are in good agreement with experiments. We also note that these insights will have implications when lattice screening is considered, since then the characteristic frequency of phonons is close to the exciton-binding energy, likely exacerbating the importance of screening dynamics. In this case, the validity of the perturbative treatment and effective screening approach is expected to be more questionable, and requires further investigation. To this end, our findings suggest that dynamical screening effects in these contexts remain a subject of future study.

[1] M. Cardona and M. L. W. Thewalt, Isotope effects on the optical spectra of semiconductors, Rev. Mod. Phys. **77**, 1173 (2005).

[2] J. Phillips, *The Fundamental Optical Spectra of Solids* (Academic Press, London, 1966), pp. 55–164.

[3] Z. H. Levine and D. C. Allan, Linear Optical Response in Silicon and Germanium Including Self-Energy Effects, Phys. Rev. Lett. **63**, 1719 (1989).

[4] M. Rohlfing and S. G. Louie, Electron-hole excitations and optical spectra from first principles, Phys. Rev. B **62**, 4927 (2000).

[5] D. M. Roundhill and J. P. Fackler Jr, *Optoelectronic Properties of Inorganic Compounds* (Springer Science & Business Media, Berlin, 1999).

[6] C. Liu and A. J. Bard, Optoelectronic properties and memories based on organic single-crystal thin films, Acc. Chem. Res. **32**, 235 (1999).

[7] P. M. Zimmerman, F. Bell, D. Casanova, and M. Head-Gordon, Mechanism for singlet fission in pentacene and tetracene: From single exciton to two triplets, J. Am. Chem. Soc. **133**, 19944 (2011).

[8] X. Wang, X. Liu, C. Cook, B. Schatschneider, and N. Marom, On the possibility of singlet fission in crystalline quaterrylene, J. Chem. Phys. **148**, 184101 (2018).

[9] J. L. Brédas and R. R. Chance, *Conjugated Polymeric Materials: Opportunities in Electronics, Optoelectronics, and Molecular Electronics* (Springer Science & Business Media, Berlin, 2012), Vol. 182.

[10] C. W. Tang, Two-layer organic photovoltaic cell, Appl. Phys. Lett. **48**, 183 (1986).

[11] W. Kohn and L. J. Sham, Self-Consistent Equations Including Exchange and Correlation Effects, Phys. Rev. **140**, A1133 (1965).

[12] P. Hohenberg and W. Kohn, Inhomogeneous Electron Gas, Phys. Rev. **136**, B864 (1964).

[13] C. C. Kim, J. W. Garland, H. Abad, and P. M. Raccah, Modeling the optical dielectric function of semiconductors: Extension of the critical-point parabolic-band approximation, Phys. Rev. B **45**, 11749 (1992).

[14] Z. H. Levine and S. G. Louie, New model dielectric function and exchange-correlation potential for semiconductors and insulators, Phys. Rev. B **25**, 6310 (1982).

[15] M. Dadsetani, H. Nejatipour, and A. Ebrahimian, *Ab initio* study of the optical properties of crystalline phenanthrene, including the excitonic effects, J. Phys. Chem. Solids **80**, 67 (2015).

[16] X. Liu, R. Tom, X. Wang, C. Cook, B. Schatschneider, and N. Marom, Pyrene-stabilized acenes as intermolecular singlet fission candidates: Importance of exciton wave-function convergence, J. Phys.: Condens. Matter. **32**, 184001 (2020).

[17] X. Wang, T. Garcia, S. Monaco, B. Schatschneider, and N. Marom, Effect of crystal packing on the excitonic properties of rubrene polymorphs, CrystEngComm **18**, 7353 (2016).

[18] F. Bechstedt, *Many-Body Approach to Electronic Excitations* (Springer, Berlin, 2016).

[19] G. Onida, L. Reining, and A. Rubio, Electronic excitations: density-functional versus many-body Green's-function approaches, Rev. Mod. Phys. **74**, 601 (2002).

[20] A. Schleife, C. Rödl, F. Fuchs, J. Furthmüller, and F. Bechstedt, Optical and energy-loss spectra of MgO, ZnO, and CdO from ab initio many-body calculations, Phys. Rev. B **80**, 035112 (2009).

[21] A. Schleife and F. Bechstedt, Ab initio description of quasiparticle band structures and optical near-edge absorption of transparent conducting oxides, J. Mater. Res. **27**, 2180 (2012).

[22] K. Kang, A. Kononov, C.-W. Lee, J. A. Leveillee, E. P. Shapera, X. Zhang, and A. Schleife, Pushing the frontiers of modeling excited electronic states and dynamics to accelerate materials engineering and design, Comput. Mater. Sci. **160**, 207 (2019).

[23] T. Sander, E. Maggio, and G. Kresse, Beyond the Tamm-Dancoff approximation for extended systems using exact diagonalization, Phys. Rev. B **92**, 045209 (2015).

[24] J. Deslippe, G. Samsonidze, D. A. Strubbe, M. Jain, M. L. Cohen, and S. G. Louie, BerkeleyGW: A massively parallel computer package for the calculation of the quasiparticle and optical properties of materials and nanostructures, Comput. Phys. Commun. **183**, 1269 (2012).

[25] D. Sangalli, A. Ferretti, H. Miranda, C. Attaccalite, I. Marri, E. Cannuccia, P. Melo, M. Marsili, F. Paleari, A. Marrazzo, G. Prandini, P. Bonfà, M. O. Atambo, F. Affinito, M. Palummo, A. Molina-Sánchez, C. Hogan, M. Grüning, D. Varsano, and A. Marini, Many-body perturbation theory calculations using the Yambo code, J. Phys.: Condens. Matter **31**, 325902 (2019).

[26] C. Vorwerk, B. Aurich, C. Cocchi, and C. Draxl, Bethe–Salpeter equation for absorption and scattering spectroscopy: Implementation in the exciting code, Electron. Struct. **1**, 037001 (2019).

[27] V. Blum, R. Gehrke, F. Hanke, P. Havu, V. Havu, X. Ren, K. Reuter, and M. Scheffler, *Ab initio* molecular simulations with numeric atom-centered orbitals, Comput. Phys. Commun. **180**, 2175 (2009).

[28] M. Giantomassi, M. Stankovski, R. Shaltaf, M. Grüning, F. Bruneval, P. Rinke, and G.-M. Rignanese, Electronic properties of interfaces and defects from many-body perturbation theory: Recent developments and applications, Phys. Status Solidi B **248**, 275 (2011).

[29] D. Y. Qiu, F. H. da Jornada, and S. G. Louie, Screening and many-body effects in two-dimensional crystals: Monolayer MoS_2, Phys. Rev. B **93**, 235435 (2016).

[30] S. Gao, Y. Liang, C. D. Spataru, and L. Yang, Dynamical excitonic effects in doped two-dimensional semiconductors, Nano Lett. **16**, 5568 (2016).

[31] B. Zhu, X. Chen, and X. Cui, Exciton binding energy of monolayer WS_2, Sci. Rep. **5**, 9218 (2015).

[32] M. M. Ugeda, A. J. Bradley, S. Shi, H. Felipe, Y. Zhang, D. Y. Qiu, W. Ruan, S. Mo, Z. Hussain, Z. Shen *et al.*, Giant bandgap renormalization and excitonic effects in a monolayer transition metal dichalcogenide semiconductor, Nat. Mater. **13**, 1091 (2014).

[33] K. Hummer and C. Ambrosch-Draxl, Oligoacene exciton binding energies: their dependence on molecular size, Phys. Rev. B **71**, 081202(R) (2005).

[34] X. Leng, H. Yin, D. Liang, and Y. Ma, Excitons and Davydov splitting in sexithiophene from first-principles many-body Green's function theory, J. Chem. Phys. **143**, 114501 (2015).

[35] X. Blase, I. Duchemin, and D. Jacquemin, The Bethe–Salpeter equation in chemistry: Relations with TD-DFT, applications and challenges, Chem. Soc. Rev. **47**, 1022 (2018).

[36] K. Shindo, Effective electron-hole interaction in shallow excitons, J. Phys. Soc. Jpn. **29**, 287 (1970).

[37] Y. Ma, M. Rohlfing, and C. Molteni, Excited states of biological chromophores studied using many-body perturbation theory: Effects of resonant-antiresonant coupling and dynamical screening, Phys. Rev. B **80**, 241405(R) (2009).

[38] B. Baumeier, D. Andrienko, Y. Ma, and M. Rohlfing, Excited states of Dicyanovinyl-Substituted oligothiophenes from Many-Body green's functions theory, J. Chem. Theory Comput. **8**, 997 (2012).

[39] Y. Ma, M. Rohlfing, and C. Molteni, Modeling the excited states of biological chromophores within many-body green's function theory, J. Chem. Theory Comput. **6**, 257 (2010).

[40] M. S. Hybertsen and S. G. Louie, Electron correlation in semiconductors and insulators: Band gaps and quasiparticle energies, Phys. Rev. B **34**, 5390 (1986).

[41] M. R. Filip, J. B. Haber, and J. B. Neaton, Phonon Screening of Excitons in Semiconductors: Halide Perovskites and Beyond, Phys. Rev. Lett. **127**, 067401 (2021).

[42] L. Hedin, New method for calculating the one-particle Green's function with application to the electron-gas problem, Phys. Rev. **139**, A796 (1965).

[43] G. Strinati, Effects of dynamical screening on resonances at inner-shell thresholds in semiconductors, Phys. Rev. B **29**, 5718 (1984).

[44] F. Fuchs, C. Rödl, A. Schleife, and F. Bechstedt, Efficient $\mathcal{O}(N^2)$ approach to solve the Bethe-Salpeter equation for excitonic bound states, Phys. Rev. B **78**, 085103 (2008).

[45] See Supplemental Material at http://link.aps.org/supplemental/10.1103/PhysRevB.107.235205 for information regarding to the derivation and simulation in this article. The supplemental material also contains Refs. [18,36] in Sec. A, Refs. [40,87–89] in Sec. B, Refs. [67,72,90,91] in Sec. C, Refs. [33,72] in Sec. D, and Ref. [44] in Sec. G.

[46] F. Bechstedt, R. Endeblein, and M. Koch, Theory of core excitons in semiconductors, Phys. Status Solidi B **99**, 61 (1980).

[47] B. Scharf, D. Van Tuan, I Žutić, and H. Dery, Dynamical screening in monolayer transition-metal dichalcogenides and its manifestations in the exciton spectrum, J. Phys.: Condens. Matter **31**, 203001 (2019).

[48] T. Bornath, D. Kremp, and M. Schlanges, Two-particle problem in a nonequilibrium many-particle system, Phys. Rev. E **60**, 6382 (1999).

[49] R. Zimmermann, Dynamical screening of the wannier exciton, Phys. Status Solidi B **48**, 603 (1971).

[50] R. Zimmermann, K. Kilimann, W. D. Kraeft, D. Kremp, and G. Röpke, Dynamical screening and self-energy of excitons in the electron–hole plasma, Phys. Status Solidi B **90**, 175 (1978).

[51] X. Wu, D. Davidović, S. Achilles, and E. Di Napoli, ChASE: A Distributed Hybrid CPU-GPU Eigensolver for Large-Scale Hermitian Eigenvalue Problems, in *Proceedings of the Platform for Advanced Scientific Computing Conference*, PASC '22 (ACM Press, New York, NY, 2022).

[52] X. Zhang, S. Achilles, J. Winkelmann, R. Haas, A. Schleife, and E. Di Napoli, Solving the Bethe-Salpeter equation on massively parallel architectures, Comput. Phys. Commun. **267**, 108081 (2021).

[53] P. H. Hahn, W. G. Schmidt, and F. Bechstedt, Bulk Excitonic Effects in Surface Optical Spectra, Phys. Rev. Lett. **88**, 016402 (2001).

[54] W. G. Schmidt, S. Glutsch, P. H. Hahn, and F. Bechstedt, Efficient $\mathcal{O}(N^2)$ method to solve the Bethe-Salpeter equation, Phys. Rev. B **67**, 085307 (2003).

[55] X. Ren, P. Rinke, C. Joas, and M. Scheffler, Random-phase approximation and its applications in computational chemistry and materials science, J. Mater. Sci. **47**, 7447 (2012).

[56] S. Botti and M. A. L. Marques, Strong Renormalization of the Electronic Band Gap due to Lattice Polarization in the GW Formalism, Phys. Rev. Lett. **110**, 226404 (2013).

[57] F. Bechstedt, R. Del Sole, G. Cappellini, and L. Reining, An efficient method for calculating quasiparticle energies in semiconductors, Solid State Commun. **84**, 765 (1992).

[58] C. Rödl, F. Fuchs, J. Furthmüller, and F. Bechstedt, Ab initio theory of excitons and optical properties for spin-polarized systems: Application to antiferromagnetic MnO, Phys. Rev. B **77**, 184408 (2008).

[59] A. Schleife, C. Rödl, J. Furthmüller, and F. Bechstedt, Electronic and optical properties of $Mg_xZn_{1-x}O$ and $Cd_xZn_{1-x}O$ from ab initio calculations, New J. Phys. **13**, 085012 (2011).

[60] S. Das, G. Shi, N. Sanders, and E. Kioupakis, Electronic and optical properties of two-dimensional α-PbO from first principles, Chem. Mater. **30**, 7124 (2018).

[61] J. Singh, D. Birkedal, V. G. Lyssenko, and J. M. Hvam, Binding energy of two-dimensional biexcitons, Phys. Rev. B **53**, 15909 (1996).

[62] M. Gajdoš, K. Hummer, G. Kresse, J. Furthmüller, and F. Bechstedt, Linear optical properties in the projector-augmented wave methodology, Phys. Rev. B **73**, 045112 (2006).

[63] G. Kresse and D. Joubert, From ultrasoft pseudopotentials to the projector augmented-wave method, Phys. Rev. B **59**, 1758 (1999).

[64] G. Kresse and J. Furthmüller, Efficient iterative schemes for *ab initio* total-energy calculations using a plane-wave basis set, Phys. Rev. B **54**, 11169 (1996).

[65] J. P. Perdew, K. Burke, and M. Ernzerhof, Generalized Gradient Approximation Made Simple, Phys. Rev. Lett. **77**, 3865 (1996).

[66] P. E. Blöchl, Projector augmented-wave method, Phys. Rev. B **50**, 17953 (1994).

[67] S. C. Capelli, A. Albinati, S. A. Mason, and B. T. M. Willis, Molecular motion in crystalline naphthalene: Analysis of multi-temperature X-ray and neutron diffraction data, J. Phys. Chem. A **110**, 11695 (2006).

[68] S. Grimme, Semiempirical GGA-type density functional constructed with a long-range dispersion correction, J. Comput. Chem. **27**, 1787 (2006).

[69] X. Zhang and A. Schleife, Nonequilibrium BN-ZnO: Optical properties and excitonic effects from first principles, Phys. Rev. B **97**, 125201 (2018).

[70] C. Wohlfarth, *Static Dielectric Constants of Pure Liquids and Binary Liquid Mixtures: Supplement to IV/6* (Springer Science & Business Media, Berlin, 2008), Vol. 17.

[71] T. Suthan, N. P. Rajesh, P. V. Dhanaraj, and C. K. Mahadevan, Growth and characterization of naphthalene single crystals grown by modified vertical Bridgman method, Spectrochim. Acta Part A **75**, 69 (2010).

[72] K. Hummer and C. Ambrosch-Draxl, Electronic properties of oligoacenes from first principles, Phys. Rev. B **72**, 205205 (2005).

[73] M. Pope and C. E. Swenberg, *Electronic Processes in Organic Crystals and Polymers* (Oxford University Press, New York, 1999), Vol. 2.

[74] P. Y. Yu and M. Cardona, *Fundamentals of Semiconductors: Physics and Materials Properties* (Springer, Berlin, 1996).

[75] D. M. Roessler and W. C. Walker, Electronic spectrum and ultraviolet optical properties of crystalline MgO, Phys. Rev. **159**, 733 (1967).

[76] R. C. Whited, C. J. Flaten, and W. C. Walker, Exciton thermoreflectance of MgO and CaO, Solid State Commun. **13**, 1903 (1973).

[77] P. Puschnig, C. Meisenbichler, and C. Draxl, Excited state properties of organic semiconductors: Breakdown of the Tamm-Dancoff approximation, arXiv:1306.3790.

[78] P. Puschnig and C. Ambrosch-Draxl, Optical absorption spectra of semiconductors and insulators including electron-hole correlations: An *ab initio* study within the LAPW method, Phys. Rev. B **66**, 165105 (2002).

[79] C. L. Braun and G. M. Dobbs, Intrinsic photoconductivity in naphthalene single crystals, J. Chem. Phys. **53**, 2718 (1970).

[80] A. Bergman and J. Jortner, Two-photon absorption spectra of crystalline naphthalene and of the naphthalene molecule in solution, Chem. Phys. Lett. **26**, 323 (1974).

[81] P. Swiderek, M. Michaud, G. Hohlneicher, and L. Sanche, Electron energy loss spectroscopy of solid naphthalene and acenaphthene: Search for the low-lying triplet states, Chem. Phys. Lett. **175**, 667 (1990).

[82] D. M. Hanson, R. Kopelman, and G. W. Robinson, Information on the Exciton Band Structure of the 1B2u State of Crystalline Naphthalene from the Variation of Energy Denominators Method, J. Chem. Phys. **51**, 212 (1969).

[83] N. Sato, H. Inokuchi, and E. A. Silinsh, Reevaluation of electronic polarization energies in organic molecular crystals, Chem. Phys. **115**, 269 (1987).

[84] A. I. Belkind and V. V. Grechov, Energy levels of polyacene crystals, Phys. Status Solidi A **26**, 377 (1974).

[85] J. Riga, J.-J. Pireaux, R. Caudano, and J. Verbist, A comparative ESCA study of the electronic structure of solid acenes: benzene, naphthalene, anthracene, and tetracene, Phys. Scr. **16**, 346 (1977).

[86] P. Larson, M. Dvorak, and Z. Wu, Role of the plasmon-pole model in the G W approximation, Phys. Rev. B **88**, 125205 (2013).

[87] N. Hamada, M. Hwang, and A. J. Freeman, Self-energy correction for the energy bands of silicon by the full-potential linearized augmented-plane-wave method: Effect of the valence-band polarization, Phys. Rev. B **41**, 3620 (1990).

[88] M. Rohlfing, P. Krüger, and J. Pollmann, Efficient scheme for GW quasiparticle band-structure calculations with applications to bulk Si and to the Si (001) − (2×1) surface, Phys. Rev. B **52**, 1905 (1995).

[89] R. W. Godby and R. J. Needs, Metal-Insulator Transition in Kohn-Sham Theory and Quasiparticle Theory, Phys. Rev. Lett. **62**, 1169 (1989).

[90] S. Curtarolo, W. Setyawan, G. L. W. Hart, M. Jahnatek, R. V. Chepulskii, R. H. Taylor, S. Wang, J. Xue, K. Yang, O. Levy *et al.*, AFLOW: An automatic framework for high-throughput materials discovery, Comput. Mater. Sci. **58**, 218 (2012).

[91] D. W. J. Cruickshank, A detailed refinement of the crystal and molecular structure of naphthalene, Acta Cryst. A **10**, 504 (1957).